PHYSICAL REVIEW D VOLUME 43, NUMBER 9 1 MAY 1991

Order-α_s corrections to observables from $p\bar{p} \to W^+X \to e^+\nu X$

Howard Baer
Physics Department, Florida State University, Tallahassee, Florida 32306

Mary Hall Reno
Department of Physics and Astronomy, University of Iowa, Iowa City, Iowa 52242
(Received 30 November 1990)

A calculation for $p\bar{p} \to W^+X \to e^+\nu X$ in the next-to-leading-logarithm approximation is presented, utilizing a combination of analytic and Monte Carlo integration techniques. The flexibility of the Monte Carlo technique allows us to present predictions for a variety of observables, while incorporating the effects of experimental cuts. In particular, we present $O(\alpha_s)$ predictions for the $p_T(e)$, transverse-mass, and lepton asymmetry distributions for $W \to e^+\nu$ events, including the effect of experimental cuts. We also show that the K factor for W-boson production is dependent upon the precise experimental cuts one uses to obtain an event sample.

I. INTRODUCTION

The discovery[1] of the $W^{\pm}$ bosons at the CERN S$p\bar{p}$S collider provided a triumphant verification of the standard model of strong and electroweak interactions.[2] At present, the study of the masses and widths of the W and Z bosons provides an opportunity for precision tests of the standard model. These experimental measurements, along with the calculation of their radiative corrections, can yield valuable information[3] on as yet undiscovered particles such as the top quark and the Higgs boson. Experiments at the CERN e^+e^- collider LEP and the SLAC Linear Collider have already determined[4] M_Z and Γ_Z to 0.03% and 0.6%, respectively. The mass and width of the W are more difficult to determine, since W is only produced at present at hadron colliders, where the subprocess energy is ill defined. Furthermore, the neutrino from $W \to e\nu$ or $\mu\nu$ is undetected, and its transverse energy is only inferred from momentum conservation.

The best value of the width Γ_W comes from the measured ratio $R=(W \to e\nu)/(Z^0 \to ee)$ observed at proton-antiproton colliders,[5] and has been found to be $\Gamma_W = 2.19 \pm 0.20$ GeV. This R ratio is relatively insensitive to $O(\alpha_s)$ corrections, since they largely cancel out in the ratio. The best value of the W mass comes from charge lepton plus neutrino transverse-mass measurements, which rise to a Jacobian peak in the vicinity of M_W. The shape of this transverse-mass distribution is relatively insensitive to details of the $O(\alpha_s)$ corrections. This technique has yielded a mass measurement by the Collider Detector at Fermilab (CDF) of $M_W = 80.0 \pm 0.6 \pm 0.2$ GeV.[6]

For most other measurements of observables associated with W production, for example , the total cross section, lepton p_T spectrum, and lepton rapidity distribution, a good understanding of QCD corrections is essential. There have appeared several calculations of QCD corrections to W production,[7] which give the $O(\alpha_s)$ enhancement to the lowest-order total cross sections. Furthermore, theoretical corrections to the W transverse-momentum distribution have been calculated both perturbatively[8] and with a resummed Sudakov-like factor,[9,10] by integrating over all of phase space. In a similar vein, an analytic computation to $O(\alpha_s)$ *including* the decay of the W^+ into the positron and neutrino has been performed,[11] which yields distributions in charged-lepton p_T and pseudorapidity η.

Each of the above higher-order calculations has only a limited range of applicability. The problem arises when an analysis requires the radiative corrections specific to the experimental cuts. Matrix elements squared including radiative corrections have ill-behaved regions due to soft and collinear singularities. These, together with the virtual contributions, are summed and factorized in analytic computations. They all suffer from the practical problem that experimental cuts cannot be incorporated because complete regions of phase space have been integrated analytically, including the region that one would "cut" in an experiment. Furthermore, one frequently wants predictions for observables other than those for which the differential cross section has been calculated. The shower Monte Carlo approach addresses the problem of cuts but the absolute normalization is specified only at the leading-log level. A third, hybrid technique which has been applied to other processes[12-14] is presented here. It incorporates aspects of both analytic and Monte Carlo approaches.

Our method here is to divide phase space into singular and nonsingular regions. The singular regions are evaluated analytically in n dimensions, with explicit soft and virtual pole cancellation, and factorization. The remainder is evaluated using Monte Carlo techniques, so experimental cuts can be implemented. The advantage of this method is that one may retain the absolute normalization of the analytic approach, but experimental cuts may also be incorporated. Furthermore, predictions for a variety of observables may be obtained just by binning the relevant quantities. A potential disadvantage is that

two parameters are introduced as a consequence of the division of phase space, but we shall show below that the final results are insensitive to the specific choice of parameters.

The calculation itself is presented in Sec. II, including analytic formulas. In Sec. III, we present results for cross sections and various observables from $p\bar{p}\to W^+X\to e^+\nu_e X$, including the positron transverse-momentum distribution and the positron angular asymmetry. We show these to lowest order, and through order α_s both with and without cuts. We also comment upon the general behavior of the "K factor" for W production. A brief summary and conclusions are presented in Sec. IV, and various cross-section formulas are contained in an Appendix.

II. CALCULATION

We begin with the lowest-order $2\to 2$ subprocess $q(p_1)+\bar{q}'(p_2)\to\bar{e}(k_1)+\nu(k_2)$. The subprocess cross section is given by

$$d\hat{\sigma}_{q\bar{q}'}^{(2\to 2)}=\frac{1}{16\pi\hat{s}}\overline{\sum}|M|^2_{\rm Born}dv \tag{2.1}$$

where

$$\overline{\sum}|M|^2_{\rm Born}=\frac{e^4|D_W(k^2)|^2}{16\sin^4\theta_W}\left\langle\frac{1}{3}\right\rangle \times 8[A_l A_q(\hat{t}_1^{\,2}+\hat{t}_2^{\,2})+B_l B_q(\hat{t}_1^{\,2}-\hat{t}_2^{\,2})] \tag{2.2}$$

is the spin and color summed and averaged squared matix element, and

$$D_W(k^2)=\frac{1}{(k^2-M_W^2)+iM_W\Gamma_W} \tag{2.3}$$

is the W propagator. We take

$$\Gamma_W=9\frac{e^2M_W}{48\pi\sin^2\theta_W}\ . \tag{2.4}$$

The constants $A_{l,q}$ and $B_{l,q}$ are combinations of vector and axial-vector couplings,

$$\begin{aligned}A_l&=A_q=(\tfrac{1}{2})^2+(-\tfrac{1}{2})^2\ ,\\ B_l&=B_q=2(\tfrac{1}{2})(-\tfrac{1}{2})\ ,\end{aligned} \tag{2.5}$$

and the Mandelstam invariants are

$$\begin{aligned}\hat{t}_1&=-2p_1\cdot k_1\ ,\\ \hat{t}_2&=-2p_2\cdot k_1\ ,\\ \hat{s}&=2p_1\cdot p_2\ ,\end{aligned} \tag{2.6}$$

and $v=1+\hat{t}_1/\hat{s}$.

The total cross section in leading-log (LL) approximation is obtained by convoluting with scale-violating parton distributions $G_{q/A}(x,M^2)$:

$$d\sigma=\sum_{a,b}\int dx_1\,dx_2\,G_{a/A}(x_1,M^2)G_{b/B}(x_2,M^2)d\hat{\sigma}_{ab}\ . \tag{2.7}$$

In leading-log approximation, an infinite sum of diagrams is calculated, but only the leading-logarithic terms are retained. The effects of these diagrams are embedded in the strong running coupling and scale-dependent parton distributions. Since the latter are calculated using collinear kinematics, the event structure is similar to that given by the lowest-order $2\to 2$ subprocess, and in particular, the W has no transverse momentum q_T.

To gain greater theoretical precision, one must include the $O(\alpha_s)$ corrections to the lowest-order hard-scattering subprocess using exact kinematics. The $O(\alpha_s)$ contribution include the $2\to 3$ annihilation ($q\bar{q}\to\bar{e}\nu g$) and Compton ($qg\to\bar{e}\nu q$ and $\bar{q}g\to\bar{e}\nu\bar{q}$) along with interference terms between loop corrections to $q\bar{q}\to\bar{e}\nu$ and the lowest-order diagram. The $2\to 3$ diagrams contain both collinear and soft singularities. The $2\to 3$ subprocesses have been calculated using dimensional regularization to isolate the infinities.[11] The collinear poles can then be factorized and absorbed into the structure functions. The soft singularities, which occur when the final-state gluon energy E_g approaches zero, cancel against infrared singularities from the loop-Born diagram interference. The corrected $2\to 2$ and $2\to 3$ matrix elements squared should be convoluted with next-leading order parton distribution functions to yield the next-to-leading-log (NLL) result.

Our approach is to divide the $2\to 3$ phase space into two regions via the introduction of two cutoffs δ_s and δ_c. If the gluon energy $E_g<\delta_s\sqrt{\hat{s}}/2$, then we evaluate the $2\to 3$ diagrams using the soft-gluon approximation, where the gluon energy is set to zero in the numerator. After integration over the soft region, the resulting poles can be explicitly canceled with those from the loop-Born interference. The remainder is then evaluated via Monte Carlo integration as part of the $2\to 2$ contribution. When $E_g>\delta_s\sqrt{\hat{s}}/2$ in the $q\bar{q}$ center-of-mass frame, the $2\to 3$ diagrams are evaluated using 3-body phase-space Monte Carlo techniques. Collinear singularities occur when initial- and final-state partons are collinear, so that denominators of propagators such as $\hat{t}=-2p_2\cdot p_3$ go to zero (here, p_3 is the final state parton four-momentum.) In this case, if $|\hat{t}|<\delta_c\hat{s}$, then the diagrams are evaluated in the leading-pole approximation. After n-dimensional integration over the final state parton, the explicit singularity can be factorized and absorbed into the structure functions, or canceled against corresponding terms from the loop-Born intereference. The remainder is evaluated as part of the $2\to 2$ contribution. If $|\hat{t}|>\delta_c\hat{s}$, then the $2\to 3$ diagrams are again evaluated by 3-body Monte Carlo methods. The equation for the differential $2\to 3$ annihilation or Compton-type parton-level cross section is

$$d\hat{\sigma}_{A,C}^{(2\to3)}=\frac{1}{2\hat{s}}\frac{1}{(2\pi)^5}\overline{\sum}|M|^2_{A,C}\delta^4(p_1+p_2-p_3-k_1-k_2)\frac{d^3k_1}{2E_1}\frac{d^3k_2}{2E_2}\frac{d^3p_3}{2E_3} \tag{2.8}$$

with the restrictions on the range of integration indicated above.

The end result of the calculation consists of two sets of weighted events corresponding to two-particle and three-particle final states. Each set of events depends on the cutoffs δ_s and δ_c. In Eqs. (A7) in the Appendix, the $2\to2$ matrix element squared including virtual and soft corrections is written explicitly. This replaces the Born matrix element squared in Eq. (2.1). Collinear remnants after factorization appear in Eqs. (A8) and (A9). The $2\to3$ matrix elements squared appear in Eqs. (A5) and (A6), and are inserted into the differential cross section in Eq. (2.8). As the cutoffs δ_s and δ_c approach zero, the sum of the weights of the three-body events approaches infinity. Likewise, the sum of the two-body event weights approaches negative infinity. The sum of two- and three-body contributions yields a finite cross section independent of the cutoffs as long as δ_s and δ_c are taken small enough so that the soft-gluon and leading-pole approximations are valid. If the cutoffs are taken to be too small, then practical convergence problems appear because one is canceling very large positive and negative contributions to the cross section. We show in Figs. 1 and 2 the sensitivity of the total cross section $\sigma(p\bar{p}\to W^+X\to e^+\nu X)$ to δ_s and δ_c at $\sqrt{s}=1.8$ TeV. In Fig. 1, δ_c is fixed at 0.001, and δ_s varies over the range from 10^{-2}–10^{-1} While the separate two- and three-body contributions vary with δ_s, the total cross section is a constant function of δ_s. Figure 2 shows the same cross section, now with δ_s fixed at 0.01 and δ_c varying over two orders of magnitude from 10^{-4} to 10^{-2}. Again, the summed cross section is essentially constant.

III. RESULTS

We show in Fig. 3 the total cross sections for $p\bar{p}\to W^+X\to e^+\nu+X$ at (a) $\sqrt{s}=0.63$ TeV and (b) $\sqrt{s}=1.8$ TeV. We assume $M_W=80.0$ GeV, and $\Gamma_W=2.04$ GeV. The plots show both the leading-log prediction and the next-to-leading-log prediction. In principle, we should use the NLL distribution functions, however, in practice we use the LL distributions. Dashed curves were obtained using the Duke-Owens set-1 parton distributions,[15] while the solid curves were obtained with Eichten-Hinchliffe-Lane-Quigg (EHLQ) set 1.[16] Both distributions assume $\Lambda_4=0.2$ GeV, and we have used the 2-loop expression for α_s throughout. The cross sections are plotted versus a variation in the factorization scale M^2 and the renormalization point μ^2. We have set these two scales equal to each other, such that $\mu^2=M^2=nM_W^2$, and plotted versus n. In leading-log approximation, one only has an order-of-magnitude estimate of the factorization and renormalization scale for a particular observable. Variation of the scale parameters thus provides some sort of estimate of the theoretical precision of the calculation. From Fig. 3(a), we see that the $O(\alpha_s)$ cross section gains only about 5% in theoretical precision over the lowest-order prediction. The main effect is the enhancement in the cross-section prediction, or K factor. The K factor varies depending on n from 1.25 to 1.31 at CERN collider energies. The cross sections of Fig. 3(a) are seen to be diminishing with an increase in the factorization scale and renormalization point. This is because W's are typically produced at parton x values of ~0.13 for $\sqrt{s}=0.63$ TeV. In this region, the valence-quark densities are di-

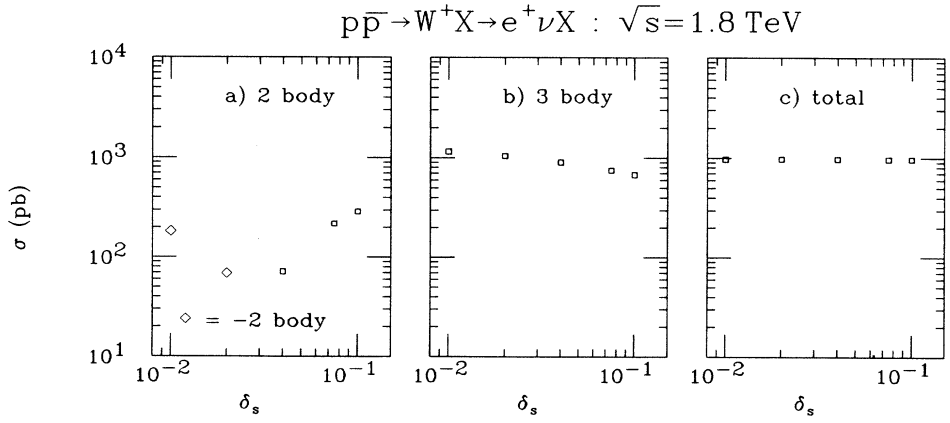

FIG. 1. Total cross section for $p\bar{p}\to W^+X\to e^+\nu X$ and $\sqrt{s}=1.8$ TeV, as a function of the cutoff δ_s. The cutoff δ_c is held constant at $\delta_c=0.001$. We have used the EHLQ set-1 distributions, and have taken $\mu^2=M^2=M_W^2$. Shown is (a) the two-body, (b) three-body, and (c) the total contribution to the cross section.

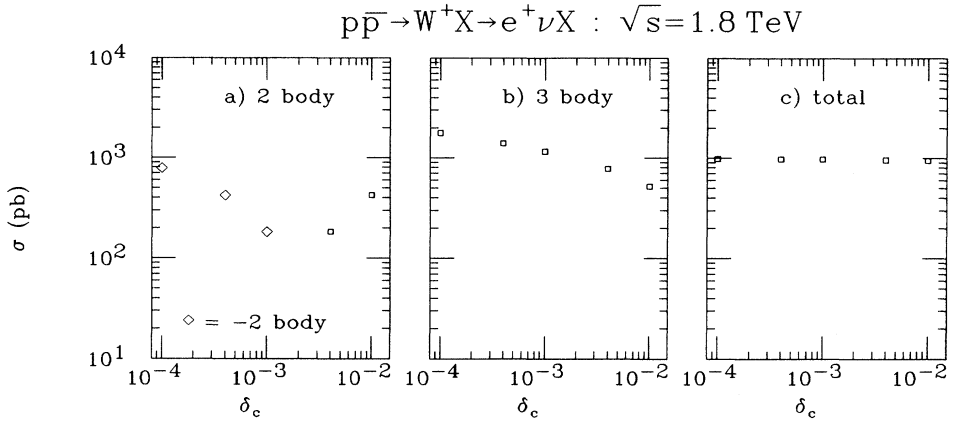

FIG. 2. Total cross section for $p\bar{p} \to W^+X \to e^+\nu X$ at $\sqrt{s} = 1.8$ TeV, as a function of the cutoff δ_c. The cutoff δ_s is held constant at $\delta_s = 0.01$. We have used the EHLQ set-1 distributions, and have taken $\mu^2 = M^2 = M_W^2$. Shown is (a) the two-body, (b) three-body, and (c) the total contribution to the cross-section.

minishing with increasing scale, while sea-quark densities at lower x are increasing. At Fermilab Tevatron collider energies, the typical parton x is ~ 0.04, where the sea quarks play a greater role. Hence, the $W \to e\nu$ cross section actually increases with increasing scale factor in Fig. 3(b). In Fig. 3(b), the variation in lowest-order prediction is about 9%, while the variation in the $O(\alpha_s)$ cross section is only 2.5%. The K factor varies depending on n from 1.22 to 1.15 at Tevatron collider energies. Hence, we see that the K factor is not really a factor, and is scale dependent, although the scale dependence for QCD corrections to electroweak processes is far less than that for processes such as dihadron production[12] or direct photon production.[14]

In Fig. 4, we show predictions for the positron transverse momentum from $W^+ \to e^+\nu_e$ events, at $\sqrt{s} = 1.8$ TeV, using the EHLQ set-1 distributions. We have invoked the following cuts used by the Collider Detector at Fermilab (CDF) Collaboration:[6] (i) $p_T(e^+) > 20$ GeV, (ii) $\not{p}_T > 20$ GeV, (iii) $|\eta_e| < 1.0$, (iv) 50 GeV $< M_T(e, \not{p}_T) < 100$ GeV, (v) no jet with $E_T > 7$ GeV anywhere in the event, and (vi) no jet with $E_T > 5$ GeV within 30° of back to back with the electromagnetic cluster, where we identify the parton energy with jet calorimeter deposition. We show for comparison the predictions at leading-log level, and predictions at next-to-leading-log level. We also show the NLL curve using the formulas of Ref. 11 with no cuts applied except that $|\eta| < 1$. The first feature

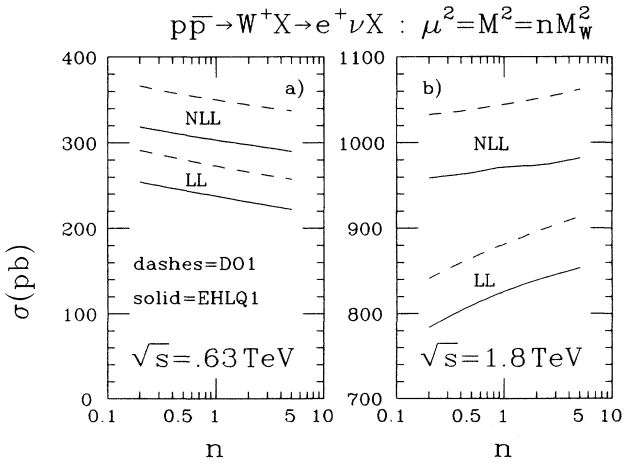

FIG. 3. Total cross section at leading log (LL) and next-to-leading-log (NLL) for $p\bar{p} \to W^+ \to e^+\nu X$ at (a) $\sqrt{s} = 0.63$ TeV, and (b) $\sqrt{s} = 1.8$ TeV, as a function of n, where $\mu^2 = M^2 = nM_W^2$. We show cross sections for DO set-1 (dashed) and EHLQ set-1 (solid) distributions.

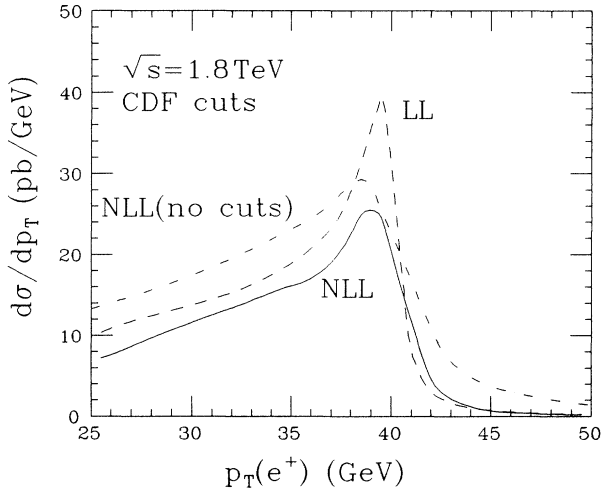

FIG. 4. Predicted transverse momentum spectrum of the positron from W^+ events at the Fermilab Tevatron. We show the NLL prediction with no cuts, and the LL and NLL predictions after imposing CDF cuts described in the text. After cuts, the ratio $\sigma_{NLL}/\sigma_{LL} = 0.88$.

worth noting is that the Jacobian peak at $\sim M_W/2$ becomes much more smeared out in going to higher order in α_s. In particular, the high-p_T tail in NLL curve is quite a bit broader due to the W transverse momentum, which does not exist in LL calculations. The NLL curve after cuts suffers some slight shape change: more events are cut out in the low-p_T region than in the peak and high-p_T region. Also, it is interesting to note that the total cut cross section actually diminishes in going from LL to NLL, the ratio being about 0.9.

In shower-model calculations of W production,[17] the total cross section is normalized by multiplying the LL cross section by the K factor. Showering off of the incoming partons then sums an infinite subset of digrams, but only at leading-log level, where the radiated gluons are assumed to be collinear; i.e., the validity of the shower becomes worse as the opening angle at which the showering occurs increases. Hence, our calculation should be more trustworthy for high-p_T W's and overall normalization, while the shower approach should provide a better description for multijet production with low-p_T W's.

In Fig. 5, we show the LL and NLL predictions for the transverse mass $M_T(e,\nu)$, after applying the above CDF cuts. In going to higher order, the high-M_T tail is diminished by only $\sim 11\%$. The peak and low-M_T tail are diminished by $\sim 20\%$ and $\sim 50\%$, respectively. The Jacobian peak at M_W maintains its position and sharpness in NLL, as expected.[18]

The CDF Collaboration has shown[19] that the lepton asymmetry can be a powerful test of structure function reliability. The asymmetry is defined as the normalized difference between the positron and electron pseudorapidity distributions from W^+ and W^- decays, respectively:

$$A(\eta)=\frac{\sigma_+(\eta)-\sigma_-(\eta)}{\sigma_+(\eta)+\sigma_-(\eta)} \ . \tag{3.1}$$

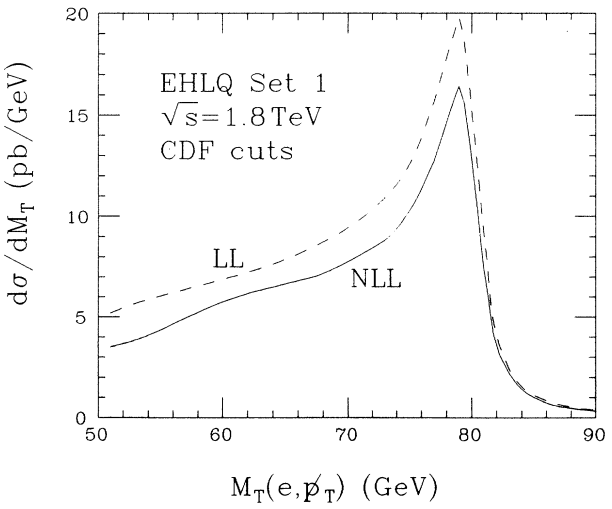

FIG. 5. Predicted transverse-mass spectrum of the positron from W events at the Fermilab Tevatron. We show the LL and NLL predictions after imposing CDF cuts described in the text.

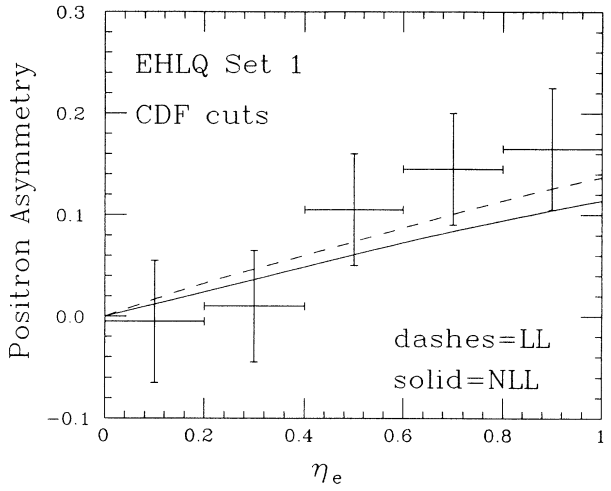

FIG. 6. Predicted distribution of positron asymmetry as a function of pseudorapidity at LL and NLL, using EHLQ set-1 parton distributions, and CDF cuts described in the text. Also shown for comparison is CDF data from Ref. 19.

Assuming CP conservation, this can also be written as

$$A(\eta)=\frac{\sigma_+(\eta)-\sigma_+(-\eta)}{\sigma_+(\eta)+\sigma_+(-\eta)} \ . \tag{3.2}$$

The CDF data favor structure functions yielding the greatest asymmetry, since the asymmetry of the data is larger than theory curves using any set of structure functions. One of the best-fitting structure functions is EHLQ set 1. The cuts used are (i) $p_T(e^+)>20$ GeV, (ii) $\not{p}_T>20$ GeV, (iii) $|\eta_e|<1.0$, (iv) 50 GeV $<M_T(e,\not{p}_T)$, and (v) no jet with $E_T>10$ GeV anywhere in the event, which are slightly different than cuts used in Figs. 4 and 5. Figure 6 shows our predictions for the positron asymmetry in lowest order (dashes) and to $O(\alpha_s)$ (solid). Also shown for comparison is the data from Ref. 19. We find that the higher-order QCD corrections actually decrease somewhat the predicted asymmetry, and thus cannot account for the slight discrepancy with the data.

IV. CONCLUDING REMARKS AND SUMMARY

One potential criticism of our calculational program is that by introducing the "no-jet" cut ($E_T^{\rm jet}<7$ GeV), the large logarithms associated with small $q_T W$'s reappear. The standard approach for W production has been to sum over polarizations and resum the large logarithms.[9,10] In the *inclusive* positron transverse-momentum spectrum, q_T is integrated, so one expects that the perturbative q_T spectrum is adequate. In the *cut* positron spectrum, the q_T scale is effectively reintroduced. We note, however, that at Tevatron energies the bulk of the discrepancy between the resummed and perturbative W q_T spectra (summed over polarizations) is below $q_T=7$ GeV.[10] Furthermore, the resummed and perturbative q_T spectra integrate to the same value for the total cross section. Consequently, we expect that the

perturbative approach is a reasonable one for the positron p_T distribution. As a check of the sensitivity of $A(\eta)$ to the jet cut, we recomputed $A(\eta)$ with a change of only the jet cut. The maximum jet E_T was changed from 7 to 20 GeV. We also computed $A(\eta)$ with no cuts. In both cases, there is little variation in $A(\eta)$ with respect to the curves in Fig. 6.

To summarize, we have used a hybrid analytic/Monte Carlo technique to compute distributions for the process $p\bar{p}\to W^+X\to e^+\nu X$, using CDF cuts for Tevatron energies, through next-to-leading order in QCD. With the NLL result, the sensitivity of the cross section to the factorization and renormalization scales is reduced. As a consequence in particular of the "no-jet" cut, we find that the positron p_T and $M_T(e,\nu)$ distributions are close in shape to the LL result, but with a lower normalization. These are specific examples of the phase-space dependence of the K factor. We have also presented the positron p_T spectrum integrated over rapidity between -1 and 1 with no cuts. The theoretical LL prediction for $A(\eta)$ with the EHLQ set-1 distributions is modified very little by the inclusion of the NLL result, so the discrepancy between the measured and LL asymmetries does not appear to be due to radiative corrections.

ACKNOWLEDGMENTS

We thank P. Arnold, E. Einsweiler, S. Errede, J. F. Owens, J. Ohnemus, and J. Stirling for discussions. M. H. R. would like to acknowledge the support of the Centro de Investigación y Estudios Avanzados del I.P.N. and Fermilab. This work was supported in part by the U.S. Department of Energy.

APPENDIX

Our notation for the momenta follows that of Aurenche and Lindfors,[11] where the subprocesses in lowest order is

$$q(p_1)+\bar{q}'(p_2)\to\bar{e}(k_1)+\nu(k_2)\ . \tag{A1}$$

In higher order, the annihilation $2\to3$ subprocess is

$$q(p_1)+\bar{q}'(p_2)\to\bar{e}(k_1)+\nu(k_2)+g(p_3) \tag{A2}$$

and the Compton-like subprocess is

$$q(p_1)+g(p_2)\to\bar{e}(k_1)+\nu(k_2)+q'(p_3)\ , \tag{A3}$$

and a similar process with q replaced by $\bar{q}$. It is convenient to define the following invariants:

$$\begin{aligned}&\hat{s}=2p_1\cdot p_2,\quad k^2=\hat{s}+\hat{t}+\hat{u}\ ,\\ &\hat{t}_1=-2p_1\cdot k_1,\quad \hat{t}=-2p_2\cdot p_3\ ,\\ &\hat{t}_2=-2p_2\cdot k_1,\quad \hat{u}=-2p_1\cdot p_3\ ,\end{aligned} \tag{A4}$$

where k^2 is the four-momentum squared of the W.

If $E_g>\delta_s\sqrt{\hat{s}}/2$, and $|\hat{t}|$ and $|\hat{u}|>\delta_c\hat{s}$, then the three-body processes are evaluated. For completeness, we reproduce the ϵ-independent squared matrix elements for the $2\to3$ subprocesses:[20] for annihilation

$$\overline{\sum}|M|^2_A=-\frac{e^4g_s^2k^2}{\sin^4\theta_W}\left\langle\frac{4}{9}\right\rangle|D_W(k^2)|^2\left[A_lA_q\left[2+\frac{\hat{s}-2\hat{t}_1-k^2}{\hat{t}}+\frac{\hat{s}-2\hat{t}_2-k^2}{\hat{u}}-2\frac{\hat{t}_1^2+\hat{t}_2^2+\hat{s}(\hat{t}_1+\hat{t}_2+k^2)}{\hat{t}\hat{u}}\right]\right.$$
$$\left.+B_lB_q\left[\frac{\hat{s}+2\hat{t}_2+k^2)}{\hat{t}}-\frac{\hat{s}+2\hat{t}_1+k^2}{\hat{u}}+2\frac{k^2(\hat{t}_1-\hat{t}_2)}{\hat{t}\hat{u}}\right]\right] \tag{A5}$$

and, for the Compton-like subprocess,

$$\overline{\sum}|M|^2_C=-\frac{e^4g_s^2k^2}{\sin^4\theta_W}\left\langle\frac{1}{6}\right\rangle|D_W(k^2)|^2\left[A_lA_q\left[\frac{\hat{t}-2(\hat{t}_1+k^2)}{\hat{s}}+\frac{\hat{s}+2(\hat{t}_1+\hat{t}_2)}{\hat{t}}+\frac{2}{\hat{s}\hat{t}}[(\hat{t}_1+\hat{t}_2+k^2)^2+\hat{t}_1^2-\hat{t}_2k^2]\right]\right.$$
$$\left.+B_lB_q\left[\frac{2(\hat{t}_1+k^2)-\hat{t}}{\hat{s}}+\frac{\hat{s}+2(\hat{t}_1+\hat{t}_2)}{\hat{t}}-\frac{2k^2(2\hat{t}_1+\hat{t}_2+k^2)}{\hat{s}\hat{t}}\right]\right] \tag{A6}$$

with A_l, A_q, B_l, and B_q as defined in Sec. II and g_s the strong coupling constant. An antiquark instead of quark in the initial state with momentum p_1 changes the sign of B_q in Eq. (A6).

The $2\to2$ contribution consists of the Born term, plus higher-order terms left over after the singularity cancellations. The two-body matrix element summed and averaged over color and spin is given by

$$\overline{\sum}|M|^2_{2\to2}=\overline{\sum}|M|^2_{\rm Born}\left\{1+\frac{\alpha_s}{2\pi}\left\langle\frac{4}{3}\right\rangle\left[-8+\pi^2+4\ln^2\delta_s+3\ln\frac{\hat{s}}{M^2}+4\ln\delta_s\ln\frac{\hat{s}}{M^2}+\lambda_{\rm FC}\left[9+\frac{2\pi^2}{3}+3\ln\delta_s-2\ln^2\delta_s\right]\right]\right\} \tag{A7}$$

where M^2 is the squared factorization scale and $\lambda_{\rm FC}$ depends on the factorization convention. We adopt the physical (deep-inelastic scattering) convention, and set $\lambda_{\rm FC}=1$.

Lastly, one must include in the $2\to2$ contribution the remnants of the collinear singularity absorption into the structure functions. These contributions are given by the remnant of $\bar{q}\to\bar{q}g$:

$$d\tilde{\sigma}_{q\bar{q}'}=\frac{\alpha_s}{2\pi}\int dx_1\,dx_2\int_{x_2}^{1-\delta_s}\frac{dz}{z}G_{\bar{q}'/B}\left[\frac{x_2}{z},M^2\right]G_{q/A}(x_1,M^2)d\hat{\sigma}_{q\bar{q}'}\left[P_{qq}(z,0)\ln\left[\delta_c\frac{\hat{s}}{M^2}\frac{1-z}{z}\right]-P'_{qq}(z,0)-\lambda_{\rm FC}f_{qq}(z)\right], \tag{A8}$$

and from $g\to q\bar{q}$, with the antiquark from the gluon annihilating the quark:

$$d\tilde{\sigma}_{qg}=\frac{\alpha_s}{2\pi}\int dx_1\,dx_2\int_{x_2}^{1}\frac{dz}{z}G_{g/B}\left[\frac{x^2}{z},M^2\right]G_{q/A}(x_1,M^2)d\hat{\sigma}_{q\bar{q}'}\left[P_{qg}(z,0)\ln\left[\delta_c\frac{\hat{s}}{M^2}\frac{1-z}{z}\right]-P'_{qg}(z,0)-\lambda_{\rm FC}f_{qG}(z)\right]. \tag{A9}$$

There are additional related terms: from q splitting into a gluon in Eq. (A8), and where the g contributes a quark rather than antiquark in Eq. (A9). As usual, there is also the swap of x_1 and x_2. The Altarelli-Parisi splitting functions for $z<1$ are

$$P_{qq}(z,0)=\left\langle\frac{4}{3}\right\rangle\left[\frac{1+z^2}{1-z}\right],\quad P_{qg}(z,0)=\tfrac{1}{2}[z^2+(1-z)^2], \tag{A10}$$

and

$$P'_{qq}(z,0)=-\left\langle\tfrac{4}{3}\right\rangle(1-z),\quad P'_{qg}(z,0)=-\tfrac{1}{2}. \tag{A11}$$

The factorization dependent terms for $z<1$ are

$$f_{qq}(z)=\left\langle\frac{4}{3}\right\rangle\left[\frac{1+z^2}{1-z}\ln\frac{1-z}{z}-\frac{3}{2}\frac{1}{1-z}+2z+3\right],\quad f_{qg}(z)=\tfrac{1}{2}\left[[z^2+(1-z)^2\ln\frac{1-z}{z}+6z(1-z)\right]. \tag{A12}$$

We have used a convention that the gluon has two spin degrees of freedom.

[1]UA1 Collaboration, G. Arnison *et al.*, Phys. Lett. **122B**, 103 (1983); **129B**, 273 (1983); UA2 Collaboration, M. Banner *et al.*, *ibid.* **122B**, 476 (1983); **129B**, 130 (1983).

[2]S. Glashow, Nucl. Phys. **22**, 579 (1961); S. Weinberg, Phys. Rev. Lett. **19**, 1264 (1967); A. Salam, in *Elementary Particle Theory: Relativistic Groups and Analyticity (Nobel Symposium No. 8)*, edited by N. Svartholm (Almqvist and Wiksell, Stockholm, 1968).

[3]U. Amaldi *et al.*, Phys. Rev. D **36**, 1385 (1987); G. Costa *et al.*, Nucl. Phys. **B297**, 244 (1988); J. Ellis and G. Fogli, Phys. Lett. B **213**, 526 (1989); F. Halzen and D. Morris, *ibid.* **237**, 107 (1990); V. Barger, J. Hewett, and T. Rizzo, Phys. Rev. Lett. **65**, 1313 (1990); R. Peccei, presented at the Beyond the Standard Model Conference, Norman, Oklahoma, 1990 (unpublished).

[4]F. Dydak, in *Proceedings of the 25th International Conference on High Energy Physics*, Singapore, 1990, edited by K. K. Phua and Y. Yamaguchi (World Scientific, Singapore, 1991).

[5]CDF Collaboration, F. Abe *et al.*, Fermilab Report No. Pub-89/245-E (unpublished).

[6]CDF Collaboration, F. Abe *et al.*, Phys. Rev. Lett. **62**, 1005 (1989); S. Errede (private communication).

[7]J. Kubar-Andre and F. Paige, Phys. Rev. D **19**, 221 (1979); G. Altarelli, R. K. Ellis, and G. Martinelli, Nucl. Phys. **B157**, 461 (1979); for a review, see the paper by S. Willenbrock, in Proceedings of the Theoretical Advanced Study Institute (TASI), Boulder, Colorado, 1989 (unpublished).

[8]P. Arnold and M. H. Reno, Nucl. Phys. **B319**, 37 (1989); **B330**, 284E (1990); R. Gonsalves, J. Pawlowski, and C. F. Wai, Phys. Rev. D **40**, 2245 (1989).

[9]G. Altarelli, R. Ellis, M. Greco, and G. Martinelli, Nucl. Phys. **B246**, 12 (1984).

[10]P. B. Arnold and R. Kaufman, Nucl. Phys. **B349**, 381 (1991).

[11]P. Aurenche and J. Lindfors, Nucl. Phys. **B185**, 274 (1981); **B185**, 301 (1981).

[12]L. Bergman, Florida State University Report No. FSU-HEP-890215 (unpublished).

[13]H. Baer, J. Ohnemus, and J. F. Owens, Phys. Rev. D **40**, 2844 (1989).

[14]H. Baer, J. Ohnemus, and J. F. Owens, Phys. Lett. B **234**, 127 (1990); Phys. Rev. D **42**, 61 (1990).

[15]D. Duke and J. F. Owens, Phys. Rev. D **30**, 49 (1984).

[16]E. Eichten, I. Hinchliffe, K. Lane, and C. Quigg, Rev. Mod. Phys. **56**, 579 (1984).

[17]T. Sjostrand, Phys. Lett. **157B**, 321 (1985); T. Gottschalk, Nucl. Phys. **B277**, 700 (1986); V. Barger, T. Gottschalk, J. Ohnemus, and R. Phillips, Phys. Rev. D **32**, 2950 (1985).

[18]V. Barger, A. Martin, and R. Phillips, Z. Phys. C **21**, 99

(1983).

[19]CDF Collaboration, J. Hauser, in *Proceedings of the Workshop on Hadron Structure Functions and Parton Distributions,* Batavia, Illinois, 1990, edited by D. F. Geesaman, J. Morfin, C. Sazama, and W. K. Tung (World Scientific, Singapore, 1990).

[20]A discussion of the treatment of γ_5 and the cancellation of order-ϵ ambiguities from the trace may be found in Ref. 11, as well as the ϵ-dependent pieces of the annihilation and Compton-like matrix elements squared.